Australian Journal of Earth Sciences (2005) **52**, (641–651)

Geology and age of the Glikson impact structure, Western Australia

F. A. MACDONALD,[1]* M. T. D. WINGATE[2] AND K. MITCHELL[3]

[1]*Division of Earth and Planetary Sciences, Harvard University, 20 Oxford Street, Cambridge, MA 02138, USA.*
[2]*Tectonics Special Research Centre, School of Earth and Geographical Sciences, University of Western Australia, 35 Stirling Highway, Crawley, WA 6009, Australia.*
[3]*81 Fern St., Gerringong, NSW 2534, Australia.*

The Glikson structure is an aeromagnetic and structural anomaly located in the Little Sandy Desert of Western Australia (23°59′S, 121°34′E). Shatter cones and planar microstructures in quartz grains are present in a highly deformed central region, suggesting an impact origin. Circumferential shortening folds and chaotically disposed bedding define a 19 km-diameter area of deformation. Glikson is located in the northwestern Officer Basin in otherwise nearly flat-lying sandstone, siltstone and conglomerate of the Neoproterozoic Mundadjini Formation, intruded by dolerite sills. The structure would not have been detected if not for its strong ring-shaped aeromagnetic anomaly, which has a 10 km inner diameter and a 14 km outer diameter. We interpret the circular magnetic signature as the product of truncation and folding of mafic sills into a ring syncline. The sills most likely correlate with dolerites that intrude the Boondawari Formation ~25 km to the north, for which we report a SHRIMP U–Pb baddeleyite and zircon age of 508 ± 5 Ma, providing a precise older limit for the impact event that formed the Glikson structure.

KEY WORDS: aeromagnetic anomalies, baddeleyite, Boondawari Formation, Glikson, impact structures, Kalkarindji Large Igneous Province, Mundadjini Formation, Officer Basin, planar microstructures, shatter cones, SHRIMP, uranium–lead dating.

INTRODUCTION

The recent widespread collection and examination of aeromagnetic data has facilitated the discovery of many terrestrial impact structures, thereby adding to the cratering record on Earth. Aeromagnetic surveys are particularly useful in Australia's vast, largely undeformed Proterozoic basins that lack substantial relief and exposure, but commonly contain highly magnetised mafic sills (Haines & Rawlings 2002). Impact processes can create magnetic anomalies by altering target rock magnetic properties (Grieve & Pilkington 1996); however, not all impacts create geophysical anomalies, and not all circular magnetic features are of impact origin. Detailed groundwork and geological studies are necessary to demonstrate an impact origin of a circular geophysical anomaly. In this contribution, we describe the results of fieldwork that indicate an impact origin of the Glikson structure, including the discovery of shatter cones. We also present a U–Pb crystallisation age for dolerites intruding into the Boondawari Formation, which, we argue, are equivalent to the disrupted dolerite sills that are responsible for the ringed magnetic anomaly.

Background

The Glikson structure is situated in the Little Sandy Desert of Western Australia at 23°59'S, 121°34′E (Figure 1), at the corner of four 1:250 000-scale geological map sheets (Bullen, Gunanya, Robertson and Trainor). Bedding attitudes marked within the structure on these maps indicate that geologists visited the area prior to 1980, but there is no mention of shocked rocks or a structural anomaly in their geological reports (Williams & Williams 1980; Leech & Brakel 1980; Tyler & Williams 1989; Williams 1992, 1995). The magnetic anomaly at Glikson (Figure 2) is so distinct that it is difficult to ascertain who was first to notice it (Tarlowski *et al.* 1993). In the mid-1990s, Alan Whitaker of Geoscience Australia pointed out the circular feature to geologist Andrew Glikson, and he in turn relayed the information to Gene and Carolyn Shoemaker, who were searching for and mapping impact structures in Australia. After a brief reconnaissance in 1996, the Shoemakers' declared that the structure was probably of impact origin and named it the Glikson structure in honour of Andrew Glikson (Shoemaker & Shoemaker 1997). Although they did not distinguish any unequivocal shock-metamorphic features, the Shoemakers were convinced of an impact origin on the basis of 'puckering' of beds,

*Corresponding author: fmacdon@fas.harvard.edu

ISSN 0812-0099 print/ISSN 1440-0952 online © Geological Society of Australia
DOI: 10.1080/08120090500170419

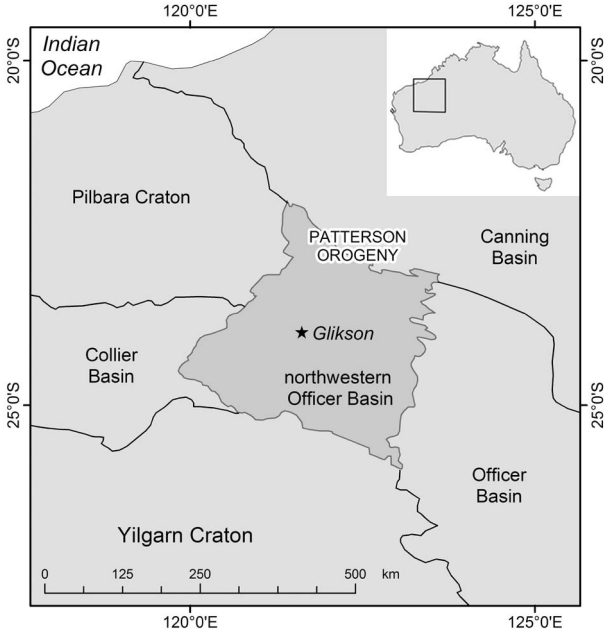

Figure 1 Location map of the Glikson impact structure in the northwestern Officer Basin, with major basins and tectonic features indicated.

characteristic of circumferential shortening associated with complex impact structures.

GEOLOGICAL SETTING

The Glikson impact structure is situated in the northwestern Officer Basin (Figure 1), a thick succession of weakly deformed, non-metamorphosed, Neoproterozoic sedimentary rocks and mafic intrusions (Williams 1992; Walter *et al.* 1994). Regionally, strata are flat-lying or gently undulating, with dips generally less than 20° (Williams & Williams 1980; Leech & Brakel 1980; Tyler & Williams 1989; Williams 1995). Regional folding and faulting was primarily related to the Patterson Orogeny, which came to a close around 550 Ma (Williams 1992; Bagas 2004). Because of its remote setting and poor exposure, the northwestern Officer Basin (previously referred to as the Savory Basin) has not been studied in great detail, and was only recently correlated with the rest of the Officer Basin (Williams 1992). More than 92% of the northwestern Officer Basin is covered by Cenozoic laterite and aeolian sand (Williams 1992). At Glikson, however, sandstone, mudstone and conglomerate of the Mundadjini Formation are exposed around the collar of the central uplift.

The Mundadjini Formation consists of siliciclastic sedimentary rocks with a maximum thickness of 1800 m (Williams 1992) and is correlated with sandstones and igneous rocks near the base of Supersequence 1 as defined by Walter *et al.* (1995) and Grey *et al.* (1999), including the Browne Formation further east in the Officer Basin and the Bitter Springs Formation of the Amadeus Basin (Grey *et al.* 1999) (Figure 3). These rocks were formed between about 840 and 800 Ma, based in part on a SHRIMP U–Pb baddeleyite and zircon age of 827 ± 6 Ma for mafic dykes of the Gairdner Dyke Swarm (Wingate *et al.* 1998), which are correlated with volcanic rocks in the Bitter Springs Formation and in the Callanna Group of the Adelaide Rift Complex (Preiss 2000; Walter *et al.* 2000).

During our fieldwork, we divided the locally exposed Mundadjini Formation into upper and lower members, separated by a 25 cm thick silty bed, although it is difficult to determine where these exposures lie within the overall Mundadjini Formation (Figure 3). The lower Mundadjini member is composed primarily of silicified sandstone with rare cross-beds. It is typically beige and weathers to form rounded blocks, unlike the more angular upper member. Some beds are conglomeratic and contain well-rounded, white, vein quartz cobbles and occasional sandstone clasts. Many cobbles exhibit closely-spaced fractures that disrupt otherwise smooth surfaces. In the Glikson structure's central region, many outcrops are deeply silicified, hindering the recognition of the original rock type. Consequently, it is possible that some or the entire lower Mundadjini member in the central region belongs to the underlying Spearhole Formation (Williams 1992) (Figure 3). The upper Mundadjini member is a medium- to coarse-grained sandstone, typically with a dark-red to purplish tone. It is more coherent than the lower member, and bedding is much easier to measure as many beds have a rather flaggy, bedding-planar fracture and some show ripple marks. The upper Mundadjini member is marked by thick sets of metre-sized, high-angle cross bedding and by several intervals of pebble conglomerate.

A few highly kaolinised dolerite outcrops occur within the Glikson structure, coincident with the aeromagnetic ring (Figure 4). Williams (1992, 1995) considered the medium- to coarse-grained intrusions in the Mundadjini and Boondawari Formations, both to the north and east of Glikson, to form a distinct group. Dolerites intruding the Boondawari Formation yielded a Rb–Sr isochron age of *ca* 640 Ma (J. R. De Laeter *in* Williams 1992). Williams (1992), however, also noted the occurrence of possibly older, fine-grained amygdaloidal sills in older strata and possibly at the base of the Mundadjini Formation (Figure 3) along the northwest margin of the northwest Officer Basin. In addition, a 50 m-thick sequence of altered amygdaloidal flows, the Keene Basalt, occurs in the *ca* 780–720 Ma Kanpa Formation (Figure 3), intersected in drillhole Lancer 1 (Haines *et al.* 2004), although Lancer 1 is about 250 km southeast of Glikson. Our preferred interpretation is that the weathered medium-grained dolerite in the outer ring of the Glikson structure correlates with other intrusions in the Mundadjini and Boondawari Formations in the area around Glikson, particularly dolerite intruding the Boondawari Formation that is exposed extensively ~25 km to the north and for which a radiometric age is reported in this paper.

Cenozoic laterite mantles the surface over the interpreted outer trough, perhaps because of slight elevation differences; however, a relationship between the magnetic anomaly and laterite exposures is not obvious, and laterite outside the structure does not have a distinctive aeromagnetic signature. Most of the region and the

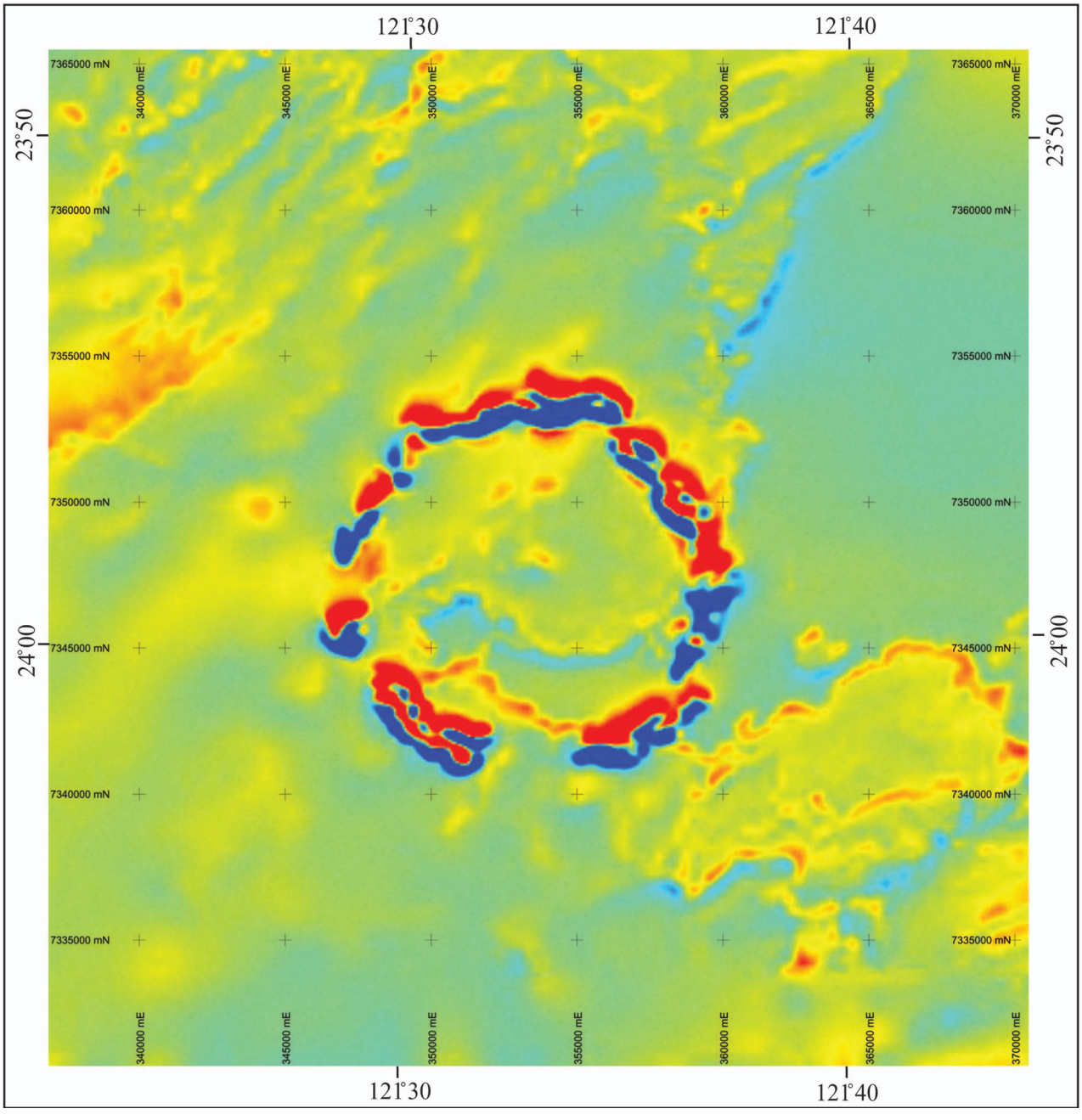

Figure 2 Regional total magnetic intensity (TMI) image of the Glikson structure, courtesy of Rio Tinto Exploration Pty Ltd and AusQuest Ltd. The line spacing of the airborne survey is 300 m and flying height 80 m MTC (mean terrain clearance). Intensity values decrease from red (highest) to dark blue (lowest). Grid ticks are spaced 5 km apart.

structure is covered by east–west-trending linear and ring sand dunes (formed by aeolian reworking of Quaternary alluvium).

GLIKSON STRUCTURE

The Glikson structure is moderately to deeply eroded, with very little circular topographic exposure. Although bedding attitudes are generally less than 20° regionally, dips within the structure are steep to nearly vertical (Figure 4). The extent of chaotically disposed bedding and arcuate truncations of the regional aeromagnetic fabric indicates that the Glikson structure has an outer diameter of 19 km (Figures 2, 4). Concentric and radial folds surround the central uplift, and a structural trough appears to be situated along the 14 km-diameter magnetic anomaly. We interpret this trough as a concealed ring syncline, and its axial position is inferred from the aeromagnetic pattern and from bedding attitudes of strata on the limbs of the fold. Within the central region, sandstone of the upper Mundadjini member is fractured and crumpled in steeply plunging folds with wavelengths ranging up to hundreds of

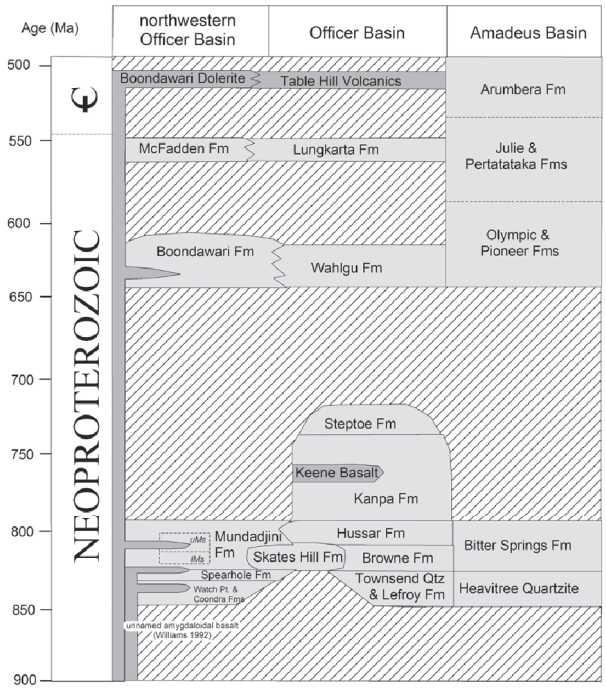

Figure 3 Stratigraphy of the northwestern Officer Basin correlated with strata of the Officer and Amadeus Basins (modified from Haines *et al.* 2004). The rocks exposed at the Glikson impact structure are shown in the Mundadjini Formation of the northwestern Officer Basin and are mapped as uMs and lMs in Figure 4.

metres. These rocks are commonly cut by closely spaced, quartz-filled fractures. Radial faults are commonly accompanied by authigenic breccias > 1 m thick; in fact, most mapped faults were initially recognised by the presence of these breccias. In the collar region, strikes tend to be tangential around the centre. Tangential linear features in the southwest are preserved in the laterite (Figure 4). This pattern of a structurally complex central region surrounded by radial and concentric folds is characteristic of circumferential shortening associated with complex impact structures (Shoemaker & Shoemaker 1996). Because strata of the central region are poorly exposed and deeply silicified, it is difficult to trace their exact position in the regional stratigraphy and thereby estimate the amount of structural uplift.

AEROMAGNETIC DATA

The Glikson structural anomaly is associated with an aeromagnetic ring anomaly that is ~ 14 km in diameter (Figure 2). This stands out prominently on regional (Bureau of Mineral Resources 1988) and national datasets (Tarlowski *et al.* 1993). Regionally, there are other ringed aeromagnetic anomalies, some of which may be impact structures (Iasky & Glikson 2004), and some may be related to igneous intrusions. Local magnetic fabric is characterised by an irregular northwest–southeast-trending mottled strip of medium-frequency anomalies that are probably related to variations in depth and thickness of mafic bodies (Williams 1995). This mottled texture continues to the north where dolerites intruding the Boondawari Formation outcrop. The very quiet aeromagnetic fabric in the northeast quadrant of Figure 2 indicates that sills may not be present in that area. The width of the Glikson aeromagnetic ring anomaly averages about 2 km, with a patchy area in the south and complexities in the east and west. The southern region is also the only place where Mundadjini Formation outcrops within the anomaly. Around the ring, discrete highs occur on the north side and lows on the south side. This is probably a skew effect from the present magnetic field interacting with surface anomalies. Along the southwest and northeast segments of the ring there is a suggestion of two distinct rings, that is, two sets of highs and lows in the 2 km strip. Inside the ring anomaly, the magnetic fabric does not appear to be markedly different from the surrounding mottled texture.

SHOCK-METAMORPHIC FEATURES

Shatter cones

During our fieldwork, only one outcrop of shatter cones was discovered. These shatter cones are formed in the upper Mundadjini member (Figure 3), ~ 3 km from the centre of the structure (Figure 4). They display strong horse-tailing with striations radiating from the apices of the cones (Figure 5). The apices of the shatter cones point roughly towards the centre of the structure, $\sim 45^{\circ}$ above the horizontal, perhaps towards the point of origin of the shock waves (Milton *et al.* 1996). The rarity of shatter cones may be due not only to the deep level of erosion, but also to the paucity of quality exposures in the central region of the structure.

Along with shatter cones, certain beds of sandstone preserve a peculiar cleavage that is reminiscent of columnar jointing. This cleavage breaks rocks into rhombic pillars with four or five sides, each with at least one slightly curved, striated surface. Where pillars are observed together they appear to form giant shatter surfaces several metres tall. This may be a peculiar form of shatter cleavage (Milton *et al.* 1996).

Planar microstructures

Thin-sections from samples of the lower member of the Mundadjini Formation in the central region of the structure commonly show planar and subplanar microstructures in quartz grains (Figure 6). Shocked quartz displays two distinct types of planar microstructures: planar fractures (PFs) and planar deformation features (PDFs) (French 1998). PFs are essentially cleavage, forming sharp, parallel sets of straight fractures with $> 15\ \mu$m spacing, while PDFs are planar, optical discontinuities of amorphous quartz, which occur in sets with $2-10\ \mu$m spacing (Haines & Rawlings 2002). The specific orientations of PDFs in a quartz grain relative to the crystallographic axis can be used to estimate the shock pressure to which the sample was subjected (French 1998).

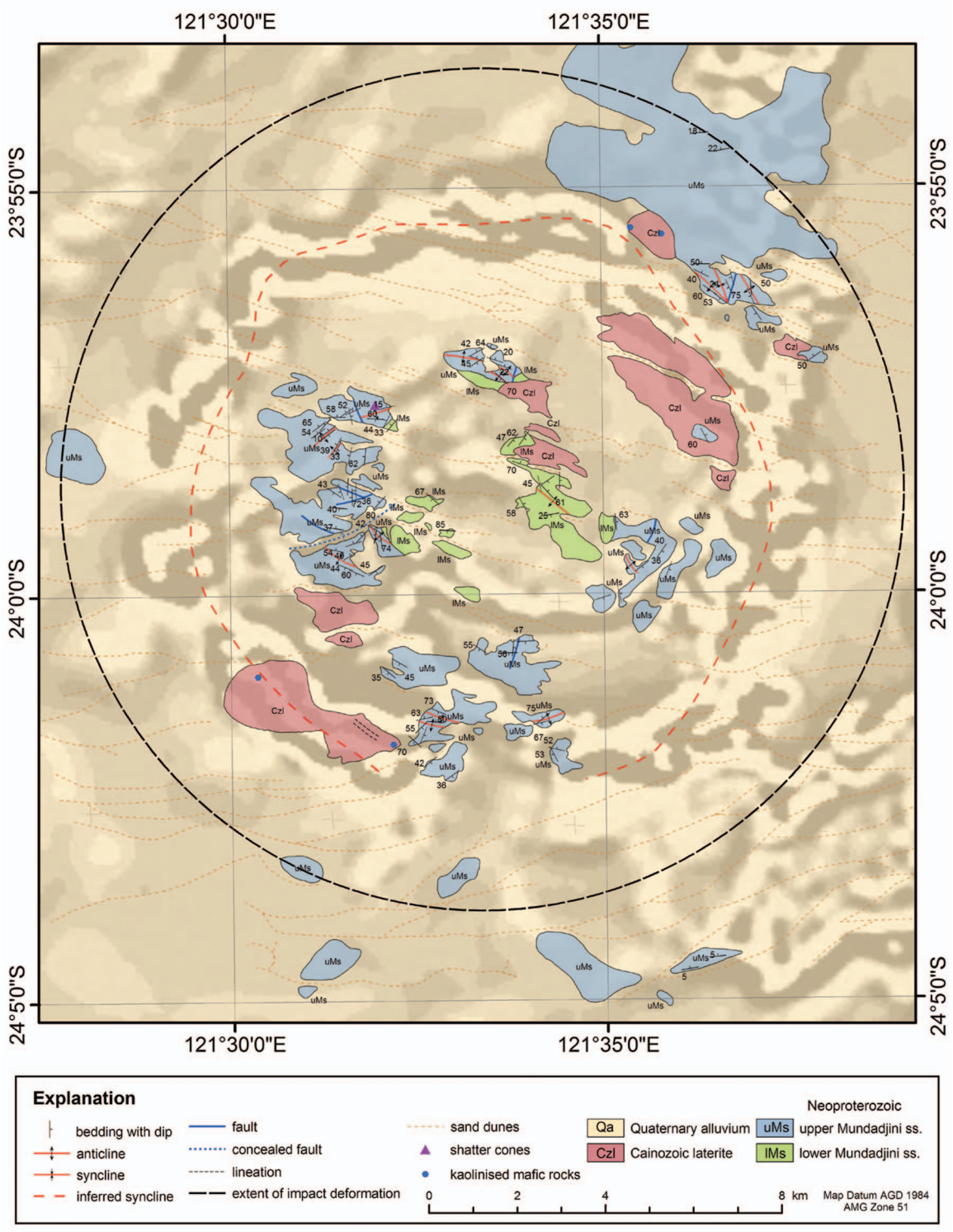

Figure 4 Geological map of the Glikson impact structure with first-derivative aeromagnetic drape in the background. The geology is by F. A. Macdonald, and the aeromagnetic image is courtesy of Rio Tinto Pty Ltd and Graeme Drew of AusQuest Ltd. Outcrops on the western collar of the central uplift and the northeast rim of the structure are excellent, whereas most other mapped outcrops are not well exposed.

At Glikson, planar microstructures in quartz grains appear to be cleavage and not true PDFs. The orientations of these disruptions are difficult to measure as the planes are commonly short and developed in small grains. Although cleavage in quartz grains has been observed frequently in association with PDFs (Kieffer 1971; Haines & Rawlings 2002), it is thought to form at lower shock pressures (< 7 GPa: Stöffler & Langenhorst 1994). The rarity or complete absence of cleavage in quartz grains in non-impact settings suggests that PFs

Figure 5 (a) Shatter cone from discovery locality (23°57.7'S, 121°32.1′E), ~3 km northwest of the centre of Glikson in the upper Mundadjini member (see Figure 4). Photo was taken facing south with hammer for scale. In the background is a counterpart of the shatter cone, pointing at approximately a 45° inclination towards the centre of the structure. (b) Close-up of the shatter cone in (a) showing the pattern of nested 'horse-tails'.

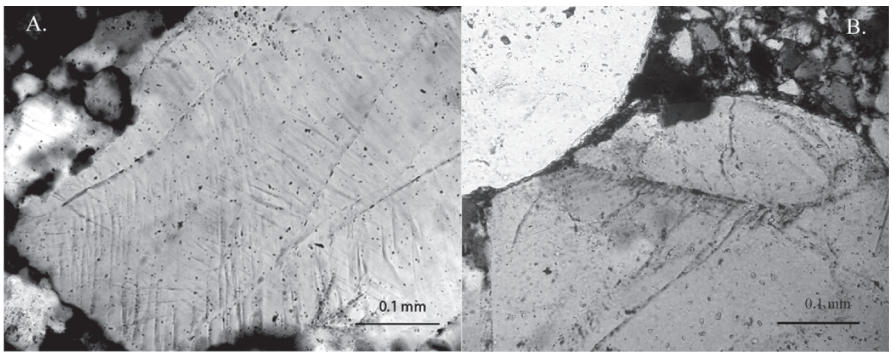

Figure 6 (a) Subplanar microstructures in quartz grains from the upper Mundadjini member, sampled ~3 km southeast of the centre of the structure (crossed polars). (b) 'Feather features' emanating from one side of a planar fracture (crossed polars). Image courtesy of Peter Haines; the sample was collected by Franco Pirajno.

can be used tentatively as an indicator of shock metamorphism (French *et al.* 2004), particularly where there exists other evidence of impact. The presence of PFs without obvious PDFs may indicate a deep level of erosion; although PDFs have been difficult to locate at many impact structures developed in sedimentary targets, such as Upheaval Dome (Kriens *et al.* 1999), Amelia Creek (Macdonald *et al.* 2005), and Rock Elm (French *et al.* 2004), and this may also reflect interstitial shock partitioning. A common type of planar microstructure in quartz grains at Glikson appears as short incipient features stemming at an angle from larger planar fractures in a feather-like pattern (Figure 5b). We believe these 'feather features' are shock damage that formed as a precursor to PDFs; similar damage in quartz grains has been seen at other probable impact structures (French *et al.* 2004). Grain mosaicism is also seen in quartz grains at Glikson (Figure 5a), and although this is not a quantitative indicator of shock pressures, mosaicism is commonly present in shocked quartz samples (Langenhorst & Deutsch 1998).

SHRIMP U–Pb GEOCHRONOLOGY OF DOLERITES INTRUDING THE BOONDAWARI FORMATION

As noted above, weathered mafic rocks in the Glikson structure most likely correlate with nearby mafic sills that intrude the Boondawari and Mundadjini Formations and outcrop extensively about 25 km north of the Glikson structure. Sample 91665 was collected from a surface exposure (23°34.5'S, 121°27.6′E) of dolerite that intrudes diamictite of the Boondawari Formation (Williams 1992). The rock is a medium- to coarse-grained, intergranular to sub-ophitic quartz dolerite, and contains plagioclase, clinopyroxene, magnetite and minor hornblende, quartz, baddeleyite and zircon. Secondary alteration includes partial saussuritisation of plagioclase and amphibole ± chlorite after pyroxene.

About 100 mainly euhedral, well-terminated zircons were separated from a 1 kg sample of dolerite using standard density and magnetic techniques. The zircons are equant to elongate (aspect ratios $\leqslant$ 3:1), and up to 250 μm long. Most are transparent and colourless to light-brown, although some are dark-brown to opaque. Euhedral concentric zoning is common. About 50

Table 1 Ion microprobe U–Th–Pb analytical data for zircon and baddeleyite from dolerite intruding the Boondawari Formation (sample 91665).

Grain	^{238}U	^{232}Th	Th/U	f_{206}	$^{206}Pb/^{238}U$		$^{207}Pb/^{206}Pb$		$^{206}Pb/^{238}U$ age		$^{207}Pb/^{206}Pb$ age	
area	(ppm)	(ppm)		(%)		($\pm 1\sigma$)		($\pm 1\sigma$)	(Ma)	($\pm 1\sigma$)	(Ma)	($\pm 1\sigma$)
Zircon												
1.1	17272	17129	0.99	0.008	0.1077	0.0025	0.05739	0.00019	659.4	14.7	506.6	7.2
2.1	10633	9342	0.88	0.017	0.1005	0.0031	0.05736	0.00026	617.6	18.4	505.4	10.0
3.1	8880	8229	0.93	0.010	0.0927	0.0009	0.05781	0.00042	571.5	5.4	522.5	15.7
4.1	8770	10169	1.16	0.007	0.0961	0.0014	0.05772	0.00050	591.7	8.1	519.3	19.0
5.1	12695	11866	0.93	0.003	0.0944	0.0015	0.05744	0.00017	581.4	8.8	508.4	6.3
6.1	3295	3372	1.02	0.023	0.0825	0.0016	0.05800	0.00042	511.2	9.8	529.9	15.8
7.1	6573	8270	1.26	0.007	0.0857	0.0015	0.05757	0.00055	530.1	8.8	513.6	21.0
8.1	4171	4686	1.12	0.013	0.0851	0.0018	0.05753	0.00022	526.3	10.8	511.7	8.4
9.1	6664	8822	1.32	0.016	0.0901	0.0043	0.05759	0.00137	556.4	25.3	514.2	51.3
10.1	4405	13204	3.00	0.008	0.0857	0.0011	0.05771	0.00113	529.9	6.5	518.9	42.2
11.1	5013	6773	1.35	0.017	0.0910	0.0018	0.05725	0.00030	561.6	10.7	501.1	11.6
12.1	1719	2527	1.47	0.017	0.0821	0.0010	0.05731	0.00033	508.6	5.9	503.3	12.5
13.1	4319	12200	2.83	0.013	0.0828	0.0005	0.05745	0.00046	512.8	3.0	509.0	17.6
14.1	5912	8899	1.51	0.007	0.0872	0.0010	0.05740	0.00013	539.0	5.8	506.8	5.0
15.1	3691	12316	3.34	0.019	0.0862	0.0009	0.05752	0.00032	533.2	5.1	511.5	12.0
16.1	8057	7845	0.97	0.017	0.0893	0.0082	0.05781	0.00159	551.2	48.3	522.4	59.2
17.1	7789	15040	1.93	0.012	0.0873	0.0018	0.05739	0.00069	539.7	10.6	506.4	26.3
18.1	2625	3779	1.44	0.001	0.0790	0.0009	0.05753	0.00025	490.1	5.4	511.9	9.7
19.1	7933	19666	2.48	0.001	0.0890	0.0014	0.05736	0.00037	549.8	8.5	505.4	14.3
20.1	9028	10705	1.19	0.017	0.0862	0.0018	0.05722	0.00061	532.9	10.4	499.8	23.4
21.1	12136	11075	0.91	0.017	0.0939	0.0020	0.05729	0.00029	578.5	11.8	502.5	11.0
22.1	12087	16375	1.35	0.002	0.0914	0.0015	0.05727	0.00027	563.8	8.7	502.0	10.4
23.1	15271	17753	1.16	0.003	0.0912	0.0015	0.05718	0.00041	562.9	9.0	498.5	15.8
24.1	9086	9792	1.08	0.017	0.0824	0.0010	0.05732	0.00032	510.3	6.2	504.1	12.2
25.1	7262	9288	1.28	0.004	0.0783	0.0012	0.05723	0.00047	485.8	7.3	500.5	17.8
26.1	13873	18120	1.31	0.006	0.0900	0.0017	0.05757	0.00034	555.3	9.8	513.3	13.1
Baddeleyite												
B1.1	341	21	0.061	0.108	0.0826	0.0010	0.05880	0.00174	511.5	6.2	559.6	63.3
B2.1	258	21	0.082	0.300	0.0771	0.0010	0.05754	0.00126	478.5	6.1	512.2	47.3
B3.1	296	11	0.036	0.029	0.0806	0.0015	0.05638	0.00072	499.6	9.1	467.3	28.0
B4.1*	216	19	0.090	11.76	0.0754	0.0048	−0.01581	0.03592	468.8	28.7	-	-
B5.1	214	12	0.054	0.195	0.0696	0.0041	0.05708	0.00121	433.6	24.9	494.7	45.9
B6.1	632	132	0.209	0.264	0.0782	0.0005	0.05583	0.00074	485.2	2.8	445.8	29.2
B7.1	265	28	0.104	0.159	0.0794	0.0028	0.05615	0.00186	492.8	16.7	458.1	71.8
B8.1*	321	70	0.220	0.583	0.0811	0.0023	0.05302	0.00294	502.7	13.5	329.8	121.1
B9.1	305	30	0.100	0.237	0.0819	0.0010	0.05729	0.00098	507.7	5.7	502.8	37.2

Notes: $f206$ is the proportion of common ^{206}Pb in measured ^{206}Pb. Isotope ratios and ages are corrected for common Pb. Uncertainties in $^{206}Pb/^{238}U$ ratios and ages do not include uncertainty (1σ) of 1.77% for zircon, 5.6% for baddeleyite, arising from calibration against the reference standard. Two analyses marked with asterisks were not included in calculation of the mean $^{207}Pb/^{206}Pb$ age for baddeleyite.

euhedral, dark-brown baddeleyite crystals, up to 50 x 150 μm, were recovered from the same sample. Zircon and baddeleyite crystals were cast, together with appropriate reference standards, in an epoxy disc, which was then polished to expose the interiors of the crystals. After thorough cleaning, the sample mount was vacuum-coated with ~500 nm Au and loaded into the SHRIMP sample lock to pump down to high vacuum for 24 hours prior to analysis.

Twenty-six zircon and nine baddeleyite grains were analysed during a single session (Table 1), using operating and data-reduction procedures for zircon and baddeleyite described by Claoué-Long *et al.* (1995) and Wingate *et al.* (1998), respectively. Absolute U and Th concentrations and $^{206}Pb/^{238}U$ ratios in zircons were determined relative to the CZ3 zircon standard [$^{206}Pb/^{238}U = 0.9142$ (564 Ma), 550 ppm ^{238}U], analyses of which were interspersed with those of zircons from the dolerites intruding the Boondawari Formation. Owing to crystal orientation effects that bias $^{206}Pb/^{238}U$ ratios measured in baddeleyite by ion microprobe (Wingate & Compston 2000), ages are based only on $^{207}Pb/^{206}Pb$ data. Accuracy of measured $^{207}Pb/^{206}Pb$ ratios was monitored by repeated analysis of the Phalaborwa baddeleyite reference standard, which has been characterised previously by both SHRIMP (Wingate 1997) and isotope dilution thermal ionisation mass spectrometric (ID-TIMS) analysis (Heaman & LeCheminant 1993). The mean $^{207}Pb/^{206}Pb$ age ($\pm 1\sigma$) for the baddeleyite standard of 2059.3 ± 3.8 Ma ($n = 8$) is indistinguishable statistically from the accepted age of 2059.8 ± 0.4 Ma. Values for ^{238}U concentration in baddeleyite are approximate, owing to large variation in ^{238}U in the Phalaborwa standard, but are proportional to true values within a single analytical session. Common Pb correction for zircon was estimated using non-radiogenic ^{204}Pb, and for badde-

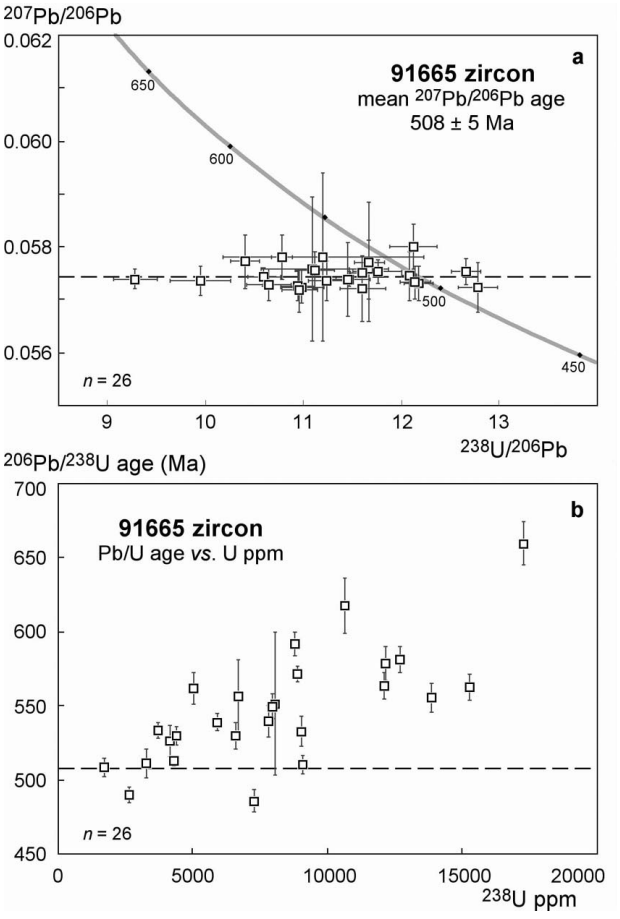

Figure 7 (a) U–Pb evolution (Concordia) diagram showing SHRIMP analytical results for zircons from dolerites intruding the Boondawari Formation (sample 91665). (b) Correlated variation between Pb/U age and U concentration.

leyite using the 208-method (Wingate *et al.* 1998), in both cases employing an average crustal common Pb composition appropriate to the age of the mineral.

The zircons are very highly enriched in U and Th. Measured ^{238}U contents range from 1700 to 17200 ppm, averaging ~8000 ppm, whereas ^{232}Th ranges from 2500 to 20 000 ppm, and averages ~10 000 ppm. Th/U ratios vary between 0.9 and 3.3, with a mean of ~1.5. Common Pb is low; the proportion of common ^{206}Pb in total ^{206}Pb (f206 in Table 1) is < 0.023% for all analyses, and averages 0.01%. Baddeleyite crystals from the same sample contain less U, from 214 to 632 ppm, with an average of ~300 ppm, Th ranges from 11 to 142 ppm, with a mean of 40 ppm, and Th/U ratios are between 0.04 and 0.22. Values for f206 are < 0.6%, averaging 0.2%, for eight analyses, and 11.8% for a single analysis, B4.1.

The ^{207}Pb/^{206}Pb ratios measured in 26 zircons agree to within analytical uncertainty and form a single, normally distributed population with a mean age of 507.8 ± 2.2 Ma (1σ, MSWD = 0.24). Corresponding ^{206}Pb/^{238}U ratios are dispersed beyond analytical precision (Figure 7a), and yield ages ranging from *ca* 660 to 485 Ma. Two analyses are slightly normally discordant, and may have undergone minor Pb loss, but the remainder are concordant to strongly reversely discordant. Good correlation is observed between apparent ^{206}Pb/^{238}U age and U concentration (Figure 7b). Reverse discordance is fairly common during SHRIMP analysis of high-U, metamict zircons (Wingate & Giddings 2000), and may be the result of enhanced sputtering of Pb relative to U due to radiation-induced microstructural changes (McLaren *et al.* 1994). The weighted mean ^{207}Pb/^{206}Pb age of 508 ± 5 Ma (95% confidence) is taken as the best estimate of the age of the zircons from the dolerite intruding the Boondawari Formation. Seven of nine baddeleyite ^{207}Pb/^{206}Pb ratios agree to within analytical uncertainty and yield a mean age of 479 ± 36 Ma. Analyses B4.1, with 11.8% common ^{206}Pb, and B8.1, which yields an imprecise age of 323 Ma, are excluded. The very high and variable U and Th content of the zircons, and agreement between baddeleyite and zircon results, indicate that the zircons formed during dyke crystallisation, hence the ^{207}Pb/^{206}Pb age of 508 ± 5 Ma obtained for the zircons is interpreted as an unambiguous age of emplacement for the dolerites intruding the Boondawari Formation.

DISCUSSION

Aeromagnetic interpretation

Because the exposed rocks in the Glikson structure consist predominantly of sandstone, the source of the circular magnetic anomaly is not immediately evident. Shoemaker and Shoemaker (1997) cited the occurrence of discrete magnetic highs north of individual magnetic lows to suggest that the anomaly is due to a chain of shallow discrete magnetised plugs or irregular intrusive bodies along an impact generated ring fault; however, their 'beads on a necklace' were an artefact of earlier datasets that sampled along east–west runs at 400 m line spacing. At higher resolution the anomaly is more continuous, with a patchy area in the south and complexities in the east and west (Figure 2). Below we assess four hypotheses to explain the formation of the Glikson magnetic anomaly.

(1) *An alkaline ring complex.* Although rare exposures of kaolinised mafic rock occur along the ring anomaly, deep weathering and poor outcrop quality hinder determination of their geochemistry and distribution. Nonetheless, the aeromagnetic image (Figure 2) hints at the subsurface geometry of the anomaly. While some ring complexes do have circular, dual-polarity magnetic anomalies (Aldrich 1986; Chandrasekhar *et al.* 2002), their magnetic signatures extend within the margins of the anomaly and are consistent with an inverted cone or plug at depth. At latitude ~25°S, an aeromagnetic image of a ring dyke should show a moderate negative anomaly on the southern segment of the ring and a strong positive anomaly on the northern segment. The magnetic anomaly at Glikson has complex and equally strong negative and positive elements with multiple strands. Moreover, an endogenic explanation is precluded by the occurrence of planar microstructures, shatter cones, and strong deformation in the central region of the Glikson structure.

(2) *An igneous intrusion along an impact-generated ring fault.* An intrusion along impact-generated weaknesses is an appealing explanation for the occurrence of these mafic rocks, the strength of the anomaly, and the preservation of a mottled fabric in the central region similar to the surrounding area, while reconciling the discovery of shock features in the central region. However, without more detailed subsurface geophysical evidence, and without other analogues on Earth of mafic intrusions along impact-generated weaknesses, with the exception of the much larger Sudbury structure (French 1998), this explanation is little more than conjectural. Furthermore, intrusions along impact-generated weaknesses are perhaps more likely to occur within the highly fractured central region.

(3) *Hydrothermal alteration and creation of highly magnetic minerals along an impact-generated fault or within a topographic trough.* An alteration hypothesis is supported by the position of the magnetic anomaly along the structural trough, the approximate coincidence of laterite with the anomaly, and the weakening in the anomaly where the upper Mundadjini member outcrops interrupt the ring. Alteration is not exclusive to either an intrusion or truncation hypothesis, and could accentuate either effect. However, if the anomaly is due entirely to alteration along impact-generated weaknesses, questions remain as to why there are no anomalies from hydrothermal alteration in the central region of the structure, and why there are no additional strong anomalies caused by alteration along tectonically generated structures in the region.

(4) *Truncation and folding of a strongly magnetised sill during an impact.* Ring magnetic anomalies have been observed at other probable impact sites in Australia, namely Shoemaker (Pirajno *et al.* 2003), Foelsche (Haines & Rawlings 2002), and Strangways (P. Haines pers. comm. 2003), and at a possible impact site, Calvert Hills (Macdonald & Mitchell 2004). The anomaly at the Shoemaker structure consists of multiple rings of high and low intensities, which Pirajno *et al.* (2003) interpreted as displacement and hydrothermal alteration of the Frere Formation. Similar to Glikson, the Foelsche and Strangways structures are located in sedimentary sequences with flat-lying mafic sills, and their magnetic anomalies have been previously explained by the removal and displacement of the pre-existing magnetic layer in the near-surface target rocks (Haines & Rawlings 2002).

If we assume that at Glikson the source of the magnetic anomaly is an originally horizontal magnetic dolerite sill, and the impact occurred after intrusion of the sill, then there would be very little magnetic signature prior to impact because TMI can only detect lateral magnetic contrasts. Moreover, if these mafic rocks are correlative with the 508 Ma dolerite intruding the Boondawari Formation, then they intruded at a time when Australia occupied low latitudes (Pisarevsky *et al.* 2001), and thus the original magnetic orientation of the sills would have been roughly parallel to the ground surface. After impact, with a normal magnetic field, a sill tilted to the north would produce a mostly negative anomaly and a sill tilted to the south would produce a positive anomaly, whereas on the east and west sides of the structure the magnetic signature would be complex. The aeromagnetic anomaly at Glikson is modelled schematically by a tabular magnetised body folded into a ring syncline (Figure 8). This model is also consistent with the complexities on the east and west segments of the ring, as these portions of the syncline are oriented obliquely to the present field. Moreover, the southwest and northeast segments of the ring anomaly appear to have two strands of dipolar features, with dominantly positive, south-dipping anomalies on the north side, and negative, north-dipping anomalies on the south side. These observations are in accord with geological mapping that suggests a syncline in this position. The weakening of the anomaly on the southern segment coincides with highly folded sandstones of the upper Mundadjini member, and is the only area in which sandstone outcrops along the anomaly. The trough of the synclinally folded dolerites may have been structurally higher on this side and was subsequently eroded away. The mottled texture within the anomaly indicates the presence of multiple sills and dykes at depth, some of which were not affected by the impact, whereas the very quiet aeromagnetic fabric in the northeast quadrant of Figure 2 is perhaps due to the absence of these sills. It is interesting to speculate whether the structure would ever have been discovered if the impact had been centred a few kilometres to the northeast, away from the magnetic sills.

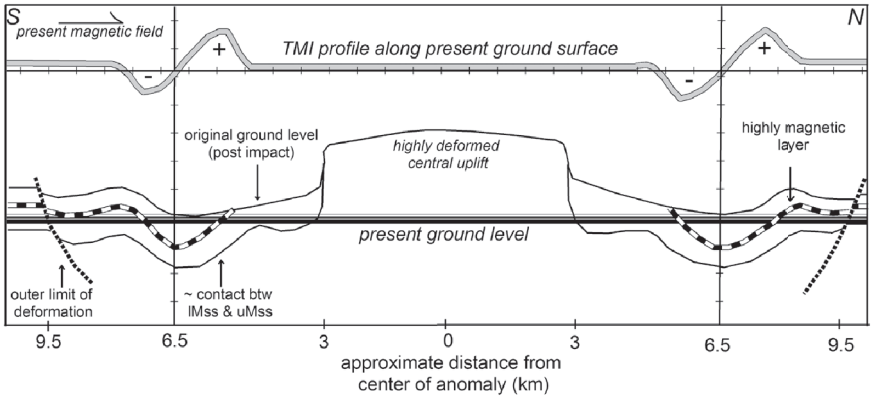

Figure 8 Model of impact deformation of a magnetised layer, erosion, and the resultant aeromagnetic pattern in a TMI profile.

We thus interpret the aeromagnetic anomaly at the Glikson structure to represent a sill that was originally at a high level, and was folded into a ring syncline by the impact. This interpretation is not independent of an effect due to the formation of magnetic mineral species by hydrothermal alteration. A syncline would also create a structural trough predisposed to alteration. Perhaps the unique combination of the folding and truncation of a magnetic layer coupled with alteration along the outer trough created the particularly strong magnetic anomaly at Glikson.

Age of the Glikson impact

A maximum age for the Glikson structure is provided by impact-deformed Mundadjini Formation, which was deposited by about 800 Ma (Preiss 2000; Haines *et al.* 2004). Provided the correlation between the 508 Ma dolerite intruding the Boondawari Formation and the strongly weathered sills in the outer ring of the Glikson structure is correct, and if our interpretation that the aeromagnetic anomaly is due to folding and truncation of these sills is also correct, then the impact occurred after 508 Ma.

Because the geological history of the northwestern Officer Basin is still poorly understood, a minimum age based on erosional history is difficult to determine. Structurally, the level of erosion is comparable to the Shoemaker structure, located in the nearby Earaheedy Basin, although Shoemaker is almost twice as large and its age is very loosely constrained (Pirajno *et al.* 2002). Circular topography at the Glikson structure is faint at best and shatter cones and other highly shocked rocks are rare; however, an outer syncline is apparently still present. These features imply an erosional compensation of the structural uplift, and a loss of strata equivalent to at least 10% of the original diameter (Grieve & Pilkington 1996). Thus, between 1 and 2 km may have been lost from the original crater. Erosion rates in the Cenozoic for arid regions of central Australia have been constrained in the Davenport Ranges (Northern Territory) to 4.5 ± 12.8 m per million years (Belton *et al.* 2004). Taking this rate implies that the impact occurred at least before Cenozoic time, and probably much earlier. We propose a post-508 Ma, Middle-to-Late Palaeozoic age for the Glikson structure.

Regional correlations

The SHRIMP U–Pb zircon age of 508 ± 5 Ma for dolerites intruding the Boondawari Formation is within uncertainty of another SHRIMP U–Pb zircon age of 513 ± 12 Ma for the Milliwindi dolerite dyke in the western Kimberley Block (Hanley & Wingate 2000). These results are also similar to a minimum 500 ± 7 Ma K–Ar age for the Table Hill Volcanics (Veevers 2000), and an Ar–Ar age of 507 ± 4 Ma for the Antrim Plateau Volcanics (Glass 2002). The Milliwindi dolerite is geochemically identical to basalts of the Antrim Plateau Volcanics, and was probably a feeder dyke for basalts that have since been eroded, implying that the Kalkarindji Large Igneous Province extended hundreds of kilometres further to the west than was recognised previously (Hanley & Wingate 2000; Glass 2002). Based on the U–Pb age alone, we suggest that the dolerite intruding the Boondawari Formation also belongs to the Kalkarindji Large Igneous Province, thereby extending the province by an additional several hundred kilometres into the northwestern Officer Basin. Independent support for this suggestion, based in part on geochemical comparisons, will be presented elsewhere (L. M. Glass pers. comm. 2004).

CONCLUSIONS

The Glikson impact structure is a ~19 km-diameter circular aeromagnetic and structural anomaly formed in Neoproterozoic strata of the northwestern Officer Basin. An impact origin is substantiated by the presence of shatter cones, planar microstructures in quartz grains, and circumferential folding around a structurally complex central region. We interpret the ringed aeromagnetic anomaly to be the result of truncation and folding of a magnetic sill into an outer syncline, and thus the impact occurred after the intrusion of this sill, which is likely correlative with 508 ± 5 Ma dolerite intruding the Boondawari Formation ~25 km north of the structure. Because the level of erosion is moderately deep, we suggest that the Glikson impact structure was formed during the Middle to Late Palaeozoic.

ACKNOWLEDGEMENTS

We thank the Geological Survey of Western Australia for use of their facilities and geophysical images. We are grateful to Ian Williams for supplying dolerite samples from the Boondawari Formation (sample 91665). We thank Franco Pirajno and Phil Hawke for extremely helpful comments on the manuscript, Peter Haines for his comments and Figure 6b, and Alastair Stewart for his thoughtful review and suggestions for Figure 8. We are grateful to Graeme Drew, Martin Gole and Jim Thornett of AusQuest for helpful discussions, and Rio Tinto Pty Ltd for use of aeromagnetic images. We thank Andrew Glikson for use of images and information, and JoAnne Gibberson for GIS help. We also thank USGS Astrogeology for use of facilities. And lastly, this work would not have been possible without support from the Thomas J. Watson Fellowship Foundation (to FAM). SHRIMP analyses were conducted at the Western Australian SHRIMP facilities, operated by a Western Australian Government–University consortium with ARC support. This is publication number 308 of the Tectonics Special Research Centre.

REFERENCES

Aldrich S. 1986. Progress report on a gravity and magnetic investigation of the Messum and Erongo igneous complexes. *Communications of the Geological Survey of South West Africa/Namibia* **2**, 47–52.

Bagas L. 2004. Proterozoic evolution and tectonic setting of the northwest Paterson Orogen, Western Australia. *Precambrian Research* **128**, 475–496.

Belton D. X., Brown R. W., Kohn B. P., Fink D. & Farley K. A. 2004. Quantitative resolution of the debate over antiquity of the central Australian landscape: implications for the tectonic and geomorphic stability of cratonic interiors. *Earth and Planetary Sciences* **219**, 21–34.

Bureau of Mineral Resources 1988. *Trainor, Total Magnetic Intensity Map, Preliminary Edition, 1:250 000 scale*. Bureau of Mineral Resources, Canberra.

Chandrasekhar D. V., Mishra D. C., Poornachandra Rao G. V. S. & Mallikharjuna Rau J. 2002. Gravity and magnetic signatures of volcanic plugs related to Deccan volcanism in Saurashra, India and their physical and geochemical properties. *Earth and Planetary Sciences* **201**, 277–292.

Claoué-Long J. C., Compston W., Roberts J. & Fanning C. M. 1995. Two Carboniferous ages: a comparison of SHRIMP zircon ages with conventional zircon ages and $^{40}Ar/^{39}Ar$ analysis. *In:* Berggren W. A., Kent D. V., Aubrey M. P. & Hardenbol J. eds. *Geochronology, Time Scales, and Global Stratigraphic Correlation*, pp. 3–21, SEPM Special Publication **54**.

French B. M. 1998. Traces of catastrophe—a handbook of shock-metamorphic effects in terrestrial meteorite impact structures. *Lunar and Planetary Science Institute, Houston, Contribution* **954**.

French B. M., Cordua W. S. & Plescia J. B. 2004. The Rock Elm meteorite impact structure, Wisconsin: geology and shock-metamorphic effects in quartz. *Geological Society of America Bulletin* **116**, 200–218.

Glass L. M. 2002. Petrogenesis and geochronology of the north Australian Kalkarinji low-Ti continental flood basalt province. PhD thesis, Australian National University, Canberra (unpubl.).

Grey K., Apak S. N., Eyles C., Eyles N., Stevens M. K. & Carlsen G. M. 1999. Neoproterozoic glaciogene successions, western Officer Basin, Western Australia. *Geological Survey of Western Australia Annual Review for 1998–1999*, 74–80.

Grieve R. A. F. & Pilkington M. 1996. The signature of terrestrial impacts. *AGSO Journal of Australian Geology & Geophysics* **16**, 399–420.

Haines P. W. & Rawlings D. J. 2002. The Foelsche structure, Northern Territory, Australia: An impact crater of probable Neoproterozoic age. *Meteoritics & Planetary Science* **37**, 269–280.

Haines P. W., Mory A. J., Stevens M. K. & Ghori K. A. R. 2004. GSWA Lancer 1 well completion report (basic data) Officer and Gunbarrel Basins, Western Australia. *Geological Survey of Western Australia Record* **2004/10**.

Hanley L. M. & Wingate M. T. D. 2000. SHRIMP zircon age for an Early Cambrian dolerite dyke: an intrusive phase of the Antrim Plateau Volcanics of northern Australia. *Australian Journal of Earth Sciences* **46**, 1029–1040.

Heaman L. M. & LeCheminant A. N. 1993. Paragenesis and U–Pb systematics of baddeleyite (ZrO_2). *Chemical Geology* **110**, 95–126.

Iasky R. & Glikson A. Y. 2004. New possible buried impact structures in the Carnarvon and Officer Basins, Western Australia. *Geological Society of Australia Abstracts* **73**, 235.

Kieffer S. W. 1971. Shock metamorphism of the Coconino Sandstone at Meteor Crater, Arizona. *Journal of Geophysical Research* **76**, 5449–5473.

Kriens B. J., Shoemaker E. M. & Herkenhoff K. E. 1999. Geology of the Upheaval Dome impact structure, southeast Utah. *Journal of Geophysical Research* **104**, 18867–18887.

Langenhorst F. & Deutsch A. 1998. Minerals in terrestrial impact structures and their characteristic features. *In:* Marfunin A.S. ed. *Advanced Mineralogy Vol. 3*, pp. 95–119. Springer, Berlin.

Leech R. E. J. & Brakel A. T. 1980. *Bullen, Western Australia, 1:250 000 Geological Series Explanatory Notes, SG 51-1*. Geological Survey of Western Australia, Perth.

Macdonald F. A., Mitchell K. & Stewart A. 2005. Amelia Creek: A Proterozoic impact structure in the Davenport Ranges, Northern Territory, Australia. *Australian Journal of Earth Sciences* **52**, 631–640.

Macdonald F. A. & Mitchell K. 2004. New possible, probable, and proven impact sites in Australia. *Geological Society of Australia Abstracts* **73**, 239.

McLaren A. C., Fitzgerald J. D. & Williams I. S. 1994. The microstructure of zircon and its influence on the age determination from Pb/U isotopic ratios measured by ion microprobe. *Geochimica et Cosmochimica Acta* **58**, 993–1005.

Milton D. J., Glikson A. Y. & Brett R. 1996. Gosses Bluff—a latest Jurassic impact structure, central Australia. Part 1: geological structure, stratigraphy, and origin. *AGSO Journal of Australian Geology & Geophysics* **16**, 453–486.

Pisarevsky S.A., Li Z. X., Grey K. & Stevens M. K. 2001. A palaeomagnetic study of Empress 1A, a stratigraphic drillhole in the Officer Basin: evidence for a low-latitude position of Australia in the Neoproterozoic. *Precambrian Research* **110**, 93–108.

Piranjo F., Hawke P., Glikson A. Y., Haines P. W. & Uysal T. 2003. Shoemaker impact structure, Western Australia. *Australian Journal of Earth Sciences* **50**, 775–796.

Preiss W. V. 2000. The Adelaide Geosyncline of South Australia and its significance in Neoproterozoic continental reconstruction. *Precambrian Research* **100**, 21–63.

Shoemaker E. M. & Shoemaker C. S. 1996. The Proterozoic impact record of Australia. *In:* Glikson A. Y. ed. *Australian Impact Structures*, pp. 379–398. AGSO Journal of Australian Geology & Geophysics **16**.

Shoemaker E. M. & Shoemaker C. S. 1997. Glikson, a probable impact structure, Western Australia. *Lunar and Planetary Science Conference XXVIII*, 1309–1310.

Stöffler D. & Langenhorst F. 1994. Shock metamorphism of quartz in nature and experiment: 1. Basic observation and theory. *Meteoritics & Planetary Science* **29**, 155–181.

Tarlowski C., Simonis F. & Milligan P. 1993. *Magnetic Anomaly Map of Australia, 1:5 000 000 scale*. Australian Geological Survey Organisation, Canberra.

Tyler I. M. & Williams I. R. 1989. *Robertson, Western Australia, 1:250 000 Geological Series Explanatory Notes, SF 51-13*. Geological Survey of Western Australia, Perth.

Veevers J. J. (Editor) 2000. *Billion-year Earth History of Australia and Neighbours in Gondwanaland*. GEMOC Press, Sydney.

Walter M. R., Grey K., Williams I. R. & Calver C. F. 1994. Stratigraphy of the Neoproterozoic to early Palaeozoic Savory Basin, Western Australia, and correlation with the Amadeus and Officer Basins. *Australian Journal of Earth Sciences* **41**, 533–546.

Walter M. R., Veevers J. J., Calver C. R. & Grey K. 1995. Neoproterozoic stratigraphy of the Centralian Superbasin, Australia. *Precambrian Research* **73**, 173–195.

Walter M. F., Veevers J. J., Calver C. R., Gorjan F. & Hill A. C. 2000. Dating the 840–544 Ma Neoproterozoic interval by isotopes of strontium, carbon, and sulfur in seawater, and some interpretive models. *Precambrian Research* **100**, 371–433.

Williams I. R. & Williams S. J. 1980. *Gunanya, Western Australia, 1:250 000 Geological Series Explanatory Notes, SF 51-14*. Geological Survey of Western Australia, Perth.

Williams I. R. 1992. Geology of the Savory Basin, Western Australia. *Geological Survey of Western Australia Bulletin* **141**.

Williams I. R. 1995. *Trainor, Western Australia, 1:250 000 Geological Series Explanatory Notes, SF 51-2*. Geological Survey of Western Australia, Perth.

Wingate M. T. D. 1997. Testing Precambrian continental reconstructions using ion microprobe U–Pb baddeleyite geochronology and paleomagnetism of mafic igneous rocks. PhD thesis, Australian National University, Canberra (unpubl.).

Wingate M. T. D., Campbell I. H., Compston W. & Gibson G. M. 1998. Ion microprobe U–Pb ages for Neoproterozoic basaltic magmatism in south-central Australia and implications for the breakup of Rodinia. *Precambrian Research* **87**, 135–159.

Wingate M. T. D. & Compston W. 2000. Crystal orientation effects during ion microprobe analysis of baddeleyite. *Chemical Geology* **168**, 75–97.

Wingate M. T. D. & Giddings J. W. 2000. Age and palaeomagnetism of the Mundine Well dyke swarm, Western Australia: implications for an Australia–Laurentia connection at 755 Ma. *Precambrian Research* **100**, 335–357.

Received 29 May 2004; accepted 7 April 2005